



Cite this: *RSC Adv.*, 2022, 12, 561

Synthesis and biological evaluation of new derivatives of thieno-thiazole and dihydrothiazolo-thiazole scaffolds integrated with a pyrazoline nucleus as anticancer and multi-targeting kinase inhibitors†

Ismail M. M. Othman,^a Zahra M. Alamshany,^b Nada Y. Tashkandi,^b Mohamed A. M. Gad-Elkareem,^a Somaia S. Abd El-Karim ^{*c} and Eman S. Nossier^d

Deregulation of various protein kinases is considered as one of the important factors resulting in cancer development and metastasis, thus multi-targeting the kinase family is one of the most important strategies in current cancer therapy. This context represents the design and synthesis of two sets of derivatives bearing a pyrazoline-3-one ring conjugated either with a thieno[3,2-*d*]thiazole or with a dihydrothiazolo[4,5-*d*]thiazole scaffold *via* an NH linker, **3a–d** and **5a–d** respectively, using the pyrazolinone–thiazolinone derivative **1** as a key precursor. All the newly synthesized compounds were assessed *in vitro* for their anticancer activity against two cancer cell lines (MCF-7 and HepG-2). The safety profile of the most active cytotoxic candidates **1** and **3c** was further examined against the normal cell line WI-38. The compounds **1** and **3c** were further evaluated as multi-targeting kinase inhibitors against EGFR, VEGFR-2 and BRAF^{V600E}, exhibiting promising suppression impact. Additionally, the latter compounds were investigated for their impact on cell cycle and apoptosis induction potential in the MCF-7 cell line. Moreover, the antimicrobial activity of all the new analogues was evaluated against a panel of Gram-positive and Gram-negative bacteria, yeast and fungi in comparison to streptomycin and amphotericin-B as reference drugs. Interestingly, both **1** and **3c** showed the most promising microbial inhibitory effect. Molecular docking studies showed promising binding patterns of the compounds **1** and **3c** with the prospective targets, EGFR, VEGFR-2 and BRAF^{V600E}. Finally, additional toxicity studies were performed for the new derivatives which showed their good drug-like properties and low toxicity risks in humans.

Received 2nd November 2021
Accepted 15th December 2021

DOI: 10.1039/d1ra08055e

rsc.li/rsc-advances

1. Introduction

Despite the extensive research and rapid progress in drug science and chemotherapeutic agents for combating cancer, it is still one of the most leading causes of death worldwide.¹ Statistics show that by 2040, cancer incidence will continue to rise to up to 29.5 million cases per year.² Cancer treatment is still a major issue, owing to the toxicity, resistance, and lack of selectivity of the currently available anticancer medications.³

Dysregulated kinase function, which typically acts as an on/off switch for cellular proliferation and motility, is considered as one of the reasons for cancer. Mutation of kinases is responsible for cellular abnormalities leading to cancer initiation, progression or metastasis.⁴ Single and multiple kinase inhibitors are now considered as targeted therapeutic strategies for human malignancy treatment.⁵ Current drug discovery research shows that PIK3CA, BRAF, VEGFR and epidermal growth factor receptor (EGFR) are key oncogenic kinase drug targets.^{5–8}

Epidermal growth factor receptor (EGFR) is a trans-membrane glycoprotein, belonging to a family which consists of four related receptor tyrosine kinases. It plays a key mediating role in cell signaling pathways including cell proliferation, apoptosis, angiogenesis, and metastatic spread.⁹ This critical role makes it a prominent target in cancer treatment. The overexpression of EGFR in a variety of human cancers, including head, neck, breast, lung, colorectal, prostate, renal, pancreas, ovary, and brain cancers results in poor treatment outcomes due to resistance to hormone therapy, cytotoxic

^aDepartment of Chemistry, Faculty of Science, Al-Azhar University, Assiut 71524, Egypt

^bDepartment of Chemistry, Faculty of Science, King Abdulaziz University, P.O. Box 42805, Jeddah 21551, Saudi Arabia

^cDepartment of Therapeutic Chemistry, National Research Centre, Dokki, Cairo 12622, Egypt. E-mail: somaia_elkarim@hotmail.com

^dDepartment of Pharmaceutical Medicinal Chemistry, Faculty of Pharmacy (Girls), Al-Azhar University, Cairo 11754, Egypt. E-mail: dremannossier@azhar.edu.eg

† Electronic supplementary information (ESI) available. See DOI: 10.1039/d1ra08055e



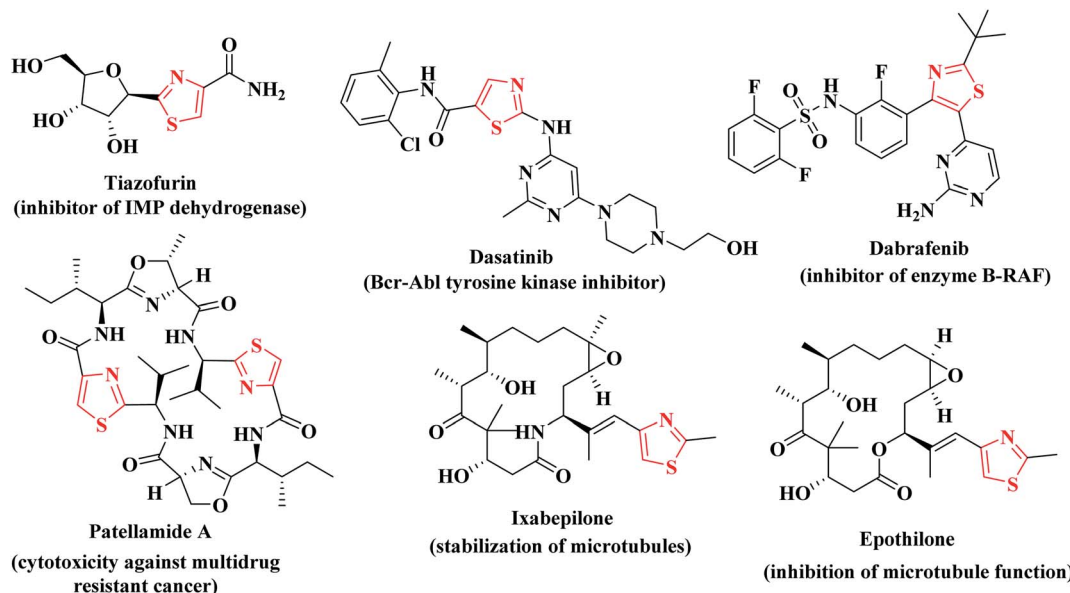


Fig. 1 Some clinically approved thiazole-bearing anticancer drugs.

drugs, and radiotherapy.^{10,11} As a result, international recommendations advocate anti-EGFR medicines as the first-line treatment in patients with advanced EGFR mutations, due to their higher efficacy and safety compared to standard chemotherapy.^{9,12,13}

Furthermore, vascular endothelial growth factor receptor-2 (VEGFR-2), a transmembrane tyrosine kinase receptor, has been identified as the most important factor in inducing angiogenesis,^{14–16} which is considered as one of the defining features of tumor growth, invasion and metastasis. VEGFR-2 has long been recognized as the most important target in cancer anti-angiogenesis therapy.^{17,18} Several small molecule VEGFR-2 inhibitors were clinically approved or evaluated for cancer treatment.^{19–21}

RAF is serine/threonine kinases which regulate ERK–MAPK pathway. There are three unique subtypes of RAF kinases in addition to homologues of BRAF.^{22–24} Many studies concluded that the BRAF serine/threonine kinase alterations have been detected in various types of human cancers that are linked to cell growth, survival and differentiation.²⁵ BRAF gene (V600E) is the most abundant type of BRAF mutation in human cancers because of substitution of a valine for glutamic acid at position 600. Current researches showed that suppression of BRAF is a new era in human cancer therapeutic treatment.²⁶

Drug discovery researches evidenced that heteroaromatic structures resemble various biologically active moieties in human bodies, like nucleic acids, hormones, and neurotransmitters. Accordingly, these scaffolds have been greatly utilized for designing different anticancer compounds which bind with different targets interrupting the biological pathways involved in cancer progress, making them as magnificent starting points for anticancer drug development.²⁷

The drug design field ensures that thiazole is the most effective motif for the said target activity. Thiazoles have

a superior anticancer activity because they have a better binding domain and less cytotoxicity in normal cells (physiological cells), but they also have site-specific mobility towards the malignant cells (pathological cell).²⁸ Additionally, thiazole derivatives were reported to exert cytotoxic potency against several types of cancer disease *via* suppression of various kinases such as; JAK2 and EGFR, VEGFR and BRAF kinases.^{29–33} In addition, different researches confirmed the potent anticancer activities of the compounds containing thiophene and thiazole heterocycles *via* inhibition of BRAF kinase activity.^{34,35} Consequently, the combined substructures (thiophene and thiazole scaffolds) may produce synergistic effects to boost the anticancer activities without compromising their original effective qualities.^{27–29} Many clinically available thiazole-bearing antiproliferative drugs have marked their presence in the field of cancer chemotherapy depicting their anticancer activity profile through diverse mechanisms such as, tiazofurin,³⁶ dasatinib,³⁷ dabrafenib,³⁸ patellamide A,³⁹ ixabepilone and epothilone^{40,41} (Fig. 1).

In addition, pyrazole heterocycle is a privileged scaffold possessing diverse biological activities.^{42,43} It is emerged as a useful pharmacophore in the synthesis of potent anticancer drugs.^{44,45} Moreover, multiple studies identified various thiazolyl-pyrazole compounds as potential anticancer agents. As an example, Lv and coworkers have reported that the thiazolyl-pyrazoline derivative **I** displayed potent cytotoxic activity against breast cancer cell line (MCF-7) with IC₅₀ of 0.07 μ M *via* EGFR inhibition with IC₅₀; 0.06 μ M.^{46,47} On the other hand, Zhao *et al.* concluded that the 4,5-dihydropyrazole derivatives bearing thiazole and thiophene moieties **IIa–c** produced effective anti-proliferative activity against WM266.4 and MCF-7 cell lines through BRAF^{V600E} inhibitory activity.⁴⁸ While Sadashiva and coworkers have investigated the dual anticancer activity against A549 and MCF-7 human cancer cell lines as well as



antimicrobial activity of the derivatives bearing thiazole heterocycle linked with pyrazoline moiety *via* carbonylhydrazone linker as compounds **IIIa–c**.⁴⁹ Furthermore, the thiazoline-pyrazolines **IV–VI** represented promising cytotoxic effects and different RTKs suppressing impact while, the thiazolopyrazolyl coumarin derivatives **VIIa, b** exhibited significant *in vitro* anticancer potentiality against different human cancer cell lines *via* a remarkable inhibition of VEGFR-2 with no noticeable toxicity towards the normal cells HFB4.⁵⁰ In addition, Vaarla *et al.* have designed and synthesized the thiazolyl-3-arylpyrazole-4-carbaldehydes **VIIIa, b** as significant antimicrobial and cytotoxic agents against HeLa cell line and the docking simulation study validated different types of interactions with human microsomal cytochrome P450 (1z11.pdb) enzyme⁵¹ (Fig. 2).

Molecular hybridization of two or more bioactive pharmacophores in the same molecular architecture represents an optimistic strategy in discovery of novel anticancer drugs. This approach raises the possibility to synergize the anticancer efficacy *via* targeting two or more molecular proteins as a single entity, reduces the risk of drug–drug interactions as well as prevents the drug resistance obstacle.⁵² Prompted by the above considerations and in view of our continuous efforts in

synthesis of heterocyclic derivatives of anticancer activity targeting different protein kinases,^{53–56} the ongoing study was focused on designing and synthesis of two sets of new analogues bearing pyrazoline-3-one ring conjugated either with the fused thieno[3,2-*d*]thiazole scaffold **3a–c** or with dihydrothiazolo[4,5-*d*]thiazole scaffold **5a–c** *via* NH linker as potential anticancer agents of multi-targeted tyrosine kinase inhibiting activity against EGFR, VEGFR-2 and BRAF^{V600E} kinases. It was taken into account the impact of molecular orientation, ring size variation and the presence of heteroatoms that could participate in hydrogen bonding interactions with the binding pockets of the protein kinases under study (Fig. 3).

All the newly synthesized compounds were assessed as anticancer candidates against human breast cancer cells (MCF-7) and human liver carcinoma cell line (HepG-2). The safety of the most promising anticancer candidates was also evaluated against the normal WI-38 cell line. Moreover, the most promising cytotoxic compounds were further evaluated as multi-targeting protein kinases against EGFR, VEGFR-2 and BRAF^{V600E} and were investigated for their impact on cell cycle and apoptosis induction potential in MCF-7 cell line.

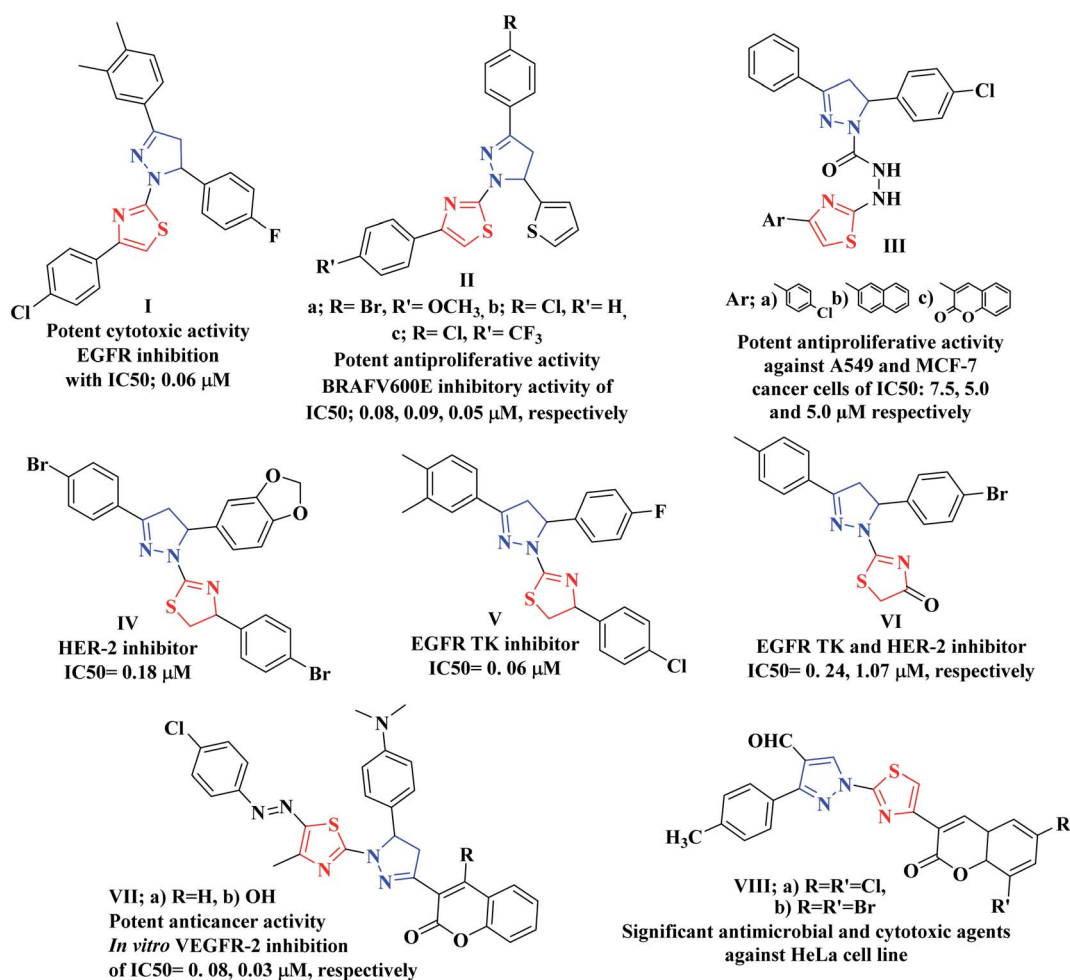


Fig. 2 Examples of various thiazolyl-pyrazoline-based compounds as anticancer candidates of TK inhibition activity.



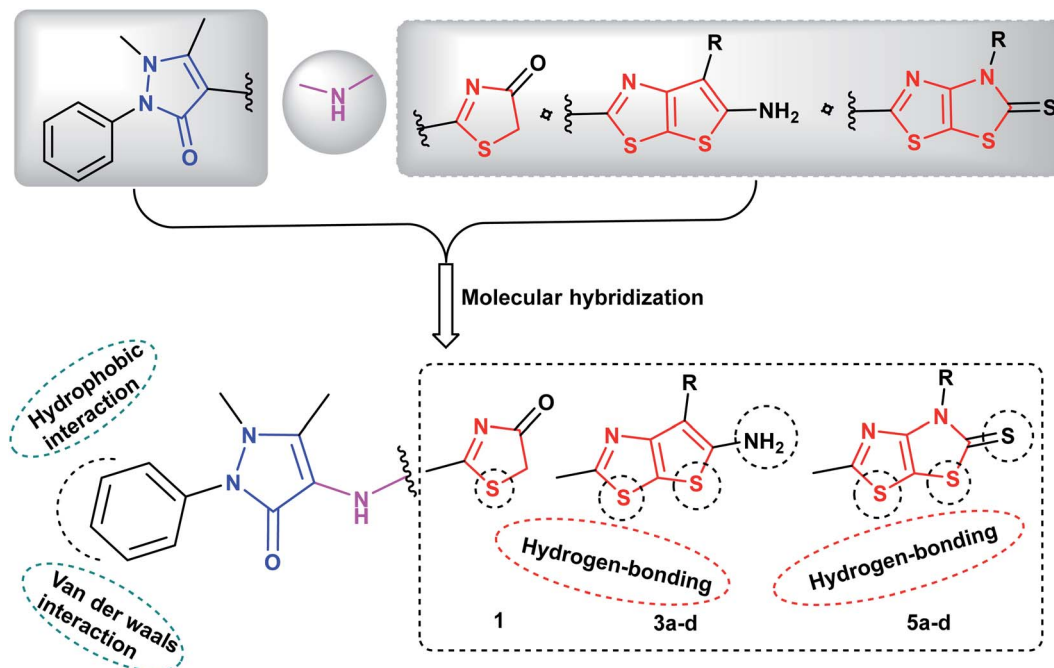


Fig. 3 Proposed hypothetical model for pyrazolyl-thieno[3,2-*d*]thiazole- and pyrazolyl-thiazolo[4,5-*d*]thiazolidine-2-thione compounds **3a-d** and **5a-d**, respectively.

Immunosuppression which usually results due to anticancer drug regimen and destruction of the mucosal barrier due to utilizing invasive devices in cancer patients make them more vulnerable to different infectious diseases that need long-term prophylactic antibiotic regimens.⁵⁷ Moreover, the efficiency of antibiotic regimen to combat infections in cancer patients is compromised due to the growth of drug resistant bacterial pathogens that dominate in neutropenic patients.⁵⁸ Accordingly, novel anticancer agents that specifically suppress cancer cells having dual anticancer and antimicrobial activities are considered to act as prophylaxis against microbial infections alongside suppressing the growth of tumors in cancer patients.^{57,58} Accordingly, the new compounds were further subjected to antimicrobial investigation in comparison to amoxicillin trihydrate and clotrimazole as standard antibacterial and antifungal drugs, respectively, against a panel of Gram-positive, Gram-negative bacterial, yeast and fungal strains. In addition, minimum inhibitory concentrations were also assessed for the new candidates. Additional toxicity study was performed for the new derivatives which represented their good drug-likeness properties and low toxicity risks in humans.

2. Experimental

2.1. Chemistry

The instruments used for measuring the melting points, spectral data (IR, mass, ¹H NMR and ¹³C NMR) and elemental analyses are provided in details in ESI.†

The chemical names given for the prepared compounds are according to the IUPAC system. 2-Chloro-*N*-(1,5-dimethyl-3-oxo-

2-phenyl-2,3-dihydro-1*H*-pyrazol-4-yl)acetamide was prepared according to the reported method.⁵⁹

2.1.1. 2-((1,5-Dimethyl-3-oxo-2-phenyl-2,3-dihydro-1*H*-pyrazol-4-yl)amino)thiazol-4(5*H*)-one (1). A mixture of 2-chloro-*N*-(1,5-dimethyl-3-oxo-2-phenyl-2,3-dihydro-1*H*-pyrazol-4-yl)acetamide (10 mmol) and ammonium thiocyanate (10 mmol) in absolute ethanol (20 mL) was refluxed for 4 h and the obtained precipitate during reflux was filtered, washed with water, dried and recrystallized from ethanol to give the title compound **1** as white crystals.

Yield 86%, mp 242–244 °C; IR ($\nu_{\max}/\text{cm}^{-1}$): 3382 (NH), 3050 (CH-arom.), 2945 (CH-aliph.), 1685, 1655 (2CO); ¹H NMR (DMSO-*d*₆) δ : 2.15 (s, 3H, CH₃), 3.21 (s, 3H, NCH₃), 4.06 (s, 2H, CH₂), 7.05–7.53 (m, 5H, Ar-H), 9.62 (s, 1H, NH, D₂O exchangeable); ¹³C NMR (DMSO-*d*₆): 12.11 (CH₃), 32.04 (CH₃), 35.16 (CH₂), 116.10, 121.07, 122.69, 128.59, 131.84, 137.91, 158.00, 166.74 (C=O), 176.13 (C=O); MS, *m/z* (%): 302 [*M*⁺] (14), 77 (100%); anal. calcd for C₁₄H₁₄N₄O₂S (302.35): C, 55.61; H, 4.67; N, 18.53; S, 10.61%. Found: C, 55.83; H, 4.89; N, 18.75; S, 10.84%.

2.1.2. General procedure for the synthesis of thieno[3,2-*d*]thiazole derivatives 3a-d. To a mixture of thiazolidin-4-one derivative **1** (10 mmol, 3.02 g) in absolute ethanol (25 mL) and dimethylformamide (2 mL) containing triethylamine (1 mL), active methylene compound **2a-d** namely; malononitrile, ethyl cyanoacetate, cyanoacetohydrazide and/or cyanothioacetamide (10 mmol) was added followed by the addition of an equimolar amount of elemental sulfur (10 mmol, 0.32 g). The reaction mixture was heated under reflux for 7 h, then cooled and neutralized by pouring onto ice/cold water containing few drops



of hydrochloric acid. The formed precipitate was filtered, dried and recrystallized from ethanol.

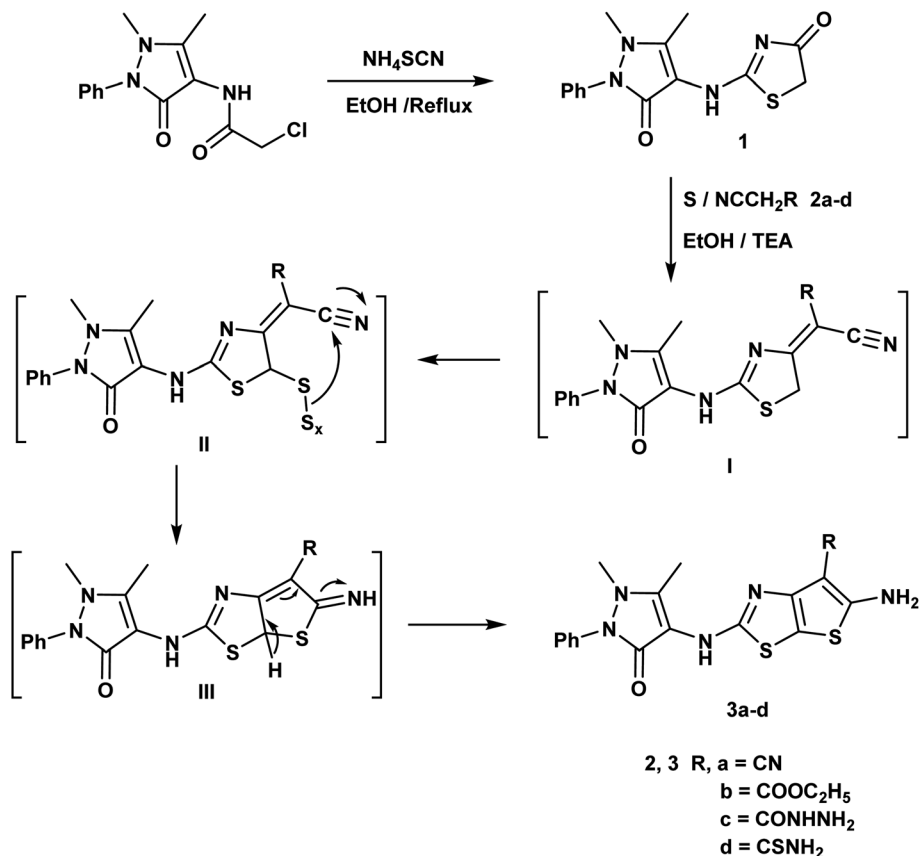
2.1.2.1. 5-Amino-2-((1,5-dimethyl-3-oxo-2-phenyl-2,3-dihydro-1H-pyrazol-4-yl)amino)thieno [3,2-d]thiazole-6-carbonitrile (3a). Yield: 72%; brown crystal; mp >300 °C; IR ($\nu_{\max}/\text{cm}^{-1}$): 3415, 3373 (NH₂), 3226 (NH), 3067 (CH-arom.), 2985 (CH-aliph.), 2212 (CN), 1658 (CO); ¹H NMR (DMSO-*d*₆) δ : 2.15 (s, 3H, CH₃), 3.07 (s, 3H, NCH₃), 6.44 (s, 2H, NH₂, D₂O exchangeable), 7.35–7.58 (m, 5H, Ar-H), 9.25 (s, 1H, NH, D₂O exchangeable); ¹³C NMR (DMSO-*d*₆): 15.62 (CH₃), 33.83 (CH₃), 106.91, 109.67, 115.86, 118.20, 120.01, 122.69, 129.60, 130.74, 135.94, 139.17, 153.27, 156.13, 165.83 (C=O); MS, *m/z* (%): 382 [M⁺] (44), 77 (100); anal. calcd for C₁₇H₁₄N₆OS₂ (382.46): C, 53.39; H, 3.69; N, 21.97; S, 16.77%. Found: C, 53.60; H, 3.89; N, 21.74; S, 16.56%.

2.1.2.2. Ethyl 5-amino-2-((1,5-dimethyl-3-oxo-2-phenyl-2,3-dihydro-1H-pyrazol-4-yl)amino)thieno[3,2-d]thiazole-6-carboxylate (3b). Yield: 75%; pale brown crystal; mp 285–287 °C; IR ($\nu_{\max}/\text{cm}^{-1}$): 3392, 3318 (NH₂), 3237 (NH), 3057 (CH-arom.), 2942 (CH-aliph.), 1715, 1654 (2CO); ¹H NMR (DMSO-*d*₆) δ : 1.23 (t, *J* = 7.2 Hz, 3H, OCH₂CH₃), 2.18 (s, 3H, CH₃), 3.11 (s, 3H, NCH₃), 4.15 (q, *J* = 7.2 Hz, 2H, CH₂, OCH₂CH₃), 6.70 (s, 2H, NH₂, D₂O exchangeable), 7.39–7.61 (m, 5H, Ar-H), 9.27 (s, 1H, NH, D₂O exchangeable); ¹³C NMR (DMSO-*d*₆): 12.35 (OCH₂CH₃), 16.24 (CH₃), 31.70 (NCH₃), 62.99 (OCH₂CH₃), 109.10, 117.58, 120.61, 123.28, 125.01, 129.42, 131.03, 134.19, 139.81, 154.38, 158.18, 165.57 (C=O), 168.73 (C=O, ester); MS,

m/z (%): 429 [M⁺] (75), 228 (100); anal. calcd for C₁₉H₁₉N₅O₃S₂ (429.52): C, 53.13; H, 4.46; N, 16.31; S, 14.93%. Found: C, 53.35; H, 4.67; N, 16.54; S, 14.72%.

2.1.2.3. 5-Amino-2-((1,5-dimethyl-3-oxo-2-phenyl-2,3-dihydro-1H-pyrazol-4-yl)amino)thieno[3,2-d]thiazole-6-carbohydrazide (3c). Yield: 70%; buff crystal; mp 293–295 °C; IR ($\nu_{\max}/\text{cm}^{-1}$): 3431, 3356, 3284, 3222 (2NH₂), 3178 (2NH), 3069 (CH-arom.), 2937 (CH-aliph.), 1698, 1652 (2CO); ¹H NMR (DMSO-*d*₆) δ : 2.21 (s, 3H, CH₃), 3.10 (s, 3H, NCH₃), 5.91 (s, 2H, NH₂, D₂O exchangeable), 7.04–7.66 (m, 8H, Ar-H, NH, NH₂, D₂O exchangeable), 9.81 (s, 1H, NH, D₂O exchangeable); ¹³C NMR (DMSO-*d*₆): 13.75 (CH₃), 33.92 (NCH₃), 109.35, 114.51, 119.71, 123.61, 129.95, 131.08, 132.52, 137.40, 139.92, 151.73, 156.24, 166.78 (C=O), 169.89 (C=O); MS, *m/z* (%): 415 [M⁺] (15), 214 (100); anal. calcd for C₁₇H₁₇N₇O₂S₂ (415.49): C, 49.14; H, 4.12; N, 23.60; S, 15.43%. Found: C, 49.35; H, 4.33; N, 23.81; S, 15.64%.

2.1.2.4. 5-Amino-2-((1,5-dimethyl-3-oxo-2-phenyl-2,3-dihydro-1H-pyrazol-4-yl)amino)thieno[3,2-d]thiazole-6-carbothioamide (3d). Yield: 73%; brown crystal; mp 297–299 °C; IR ($\nu_{\max}/\text{cm}^{-1}$): 3423, 3381, 3276, 3215 (2NH₂), 3155 (NH), 3070 (CH-arom.), 2943 (CH-aliph.), 1661 (CO); ¹H NMR (DMSO-*d*₆) δ : 2.09 (s, 3H, CH₃), 3.16 (s, 3H, NCH₃), 6.82 (s, 2H, NH₂, D₂O exchangeable), 7.53–7.99 (m, 7H, Ar-H, NH₂), 9.78 (s, 1H, NH, D₂O exchangeable); ¹³C NMR (DMSO-*d*₆): 12.42 (CH₃), 32.37 (NCH₃), 111.66, 117.31, 119.25, 121.95, 123.45, 129.61, 130.11, 132.93, 137.12, 151.32, 154.20, 165.52 (C=O), 183.72 (C=S);



Scheme 1 Synthesis of thienothiazole derivatives.





© 2022 The Author(s). Published by the Royal Society of Chemistry

($\nu_{\max}/\text{cm}^{-1}$): 3328 (NH), 3074 (CH-arom.), 2983 (CH-aliph.), 1652 (CO), 1261 (C=S); ^1H NMR (DMSO- d_6) δ : 2.27 (s, 3H, CH₃), 3.05 (s, 3H, NCH₃), 3.06 (s, 3H, NCH₃), 7.33–7.68 (m, 5H, Ar-H), 10.14 (s, 1H, NH, D₂O exchangeable); ^{13}C NMR (DMSO- d_6): 11.89 (CH₃), 31.74 (NCH₃), 34.38 (NCH₃), 117.01, 121.82, 123.94, 128.43, 131.24, 138.42, 143.51, 150.29, 158.32, 165.06 (C=O), 187.76 (C=S); MS, m/z (%): 389 [M^+] (55), 188 (100); anal. calcd for C₁₆H₁₅N₅OS₃ (389.52): C, 49.34; H, 3.88; N, 17.35; S, 24.70%. Found: C, 49.56; H, 3.67; N, 17.76; S, 24.91%.

2.1.3.4. 4-((4-(4-Chlorophenyl)-5-thioxo-4,5-dihydrothiazolo [4,5-d]thiazol-2-yl)amino)-1,5-dimethyl-2-phenyl-1H-pyrazol-3(2H)-one (**5d**). Yield: 69%; brown crystal; mp 211–213 °C; IR ($\nu_{\max}/\text{cm}^{-1}$): 3320 (NH), 3089 (CH-arom.), 2943 (CH-aliph.), 1662 (CO), 1287 (C=S); ^1H NMR (DMSO- d_6) δ : 2.12 (s, 3H, CH₃), 3.02 (s, 3H, NCH₃), 6.98 (d, J = 12.9 Hz, 2H, Ar-H), 7.29–7.34 (m, 1H, Ar-H), 7.52–7.78 (m, 6H, Ar-H), 9.43 (s, 1H, NH, D₂O exchangeable); ^{13}C NMR (DMSO- d_6): 12.18 (CH₃), 32.86 (NCH₃),

119.81, 122.42, 125.11, 128.02, 129.22, 130.16, 131.06, 133.82, 138.45, 141.73, 145.51, 158.18, 161.92, 165.87 (C=O), 183.79 (C=S); MS, m/z (%): 487, 485 [M^+] (25, 70), 202 (100); anal. calcd for C₂₁H₁₆ClN₅OS₃ (486.03): C, 51.89; H, 3.32; Cl, 7.29; N, 14.41; S, 19.79%. Found: C, 51.68; H, 3.55; Cl, 7.51; N, 14.63; S, 19.58%.

2.2. Biological activity

2.2.1. *In vitro* anticancer screening. The cell lines were purchased from the American Type Culture collection as follows: liver carcinoma cell line (HepG-2) and breast carcinoma cell line (MCF-7). Cytotoxic activity screening was performed using MTT assay at Regional Center for Mycology and Biotechnology, Al-Azhar University.⁶⁰ More details in the ESI.†

2.2.2. EGFR, VEGFR and BRAF^{V600E} kinase inhibitory assay. The most active cytotoxic compounds that showed promising IC₅₀ values against **1**, **3c** were further examined for

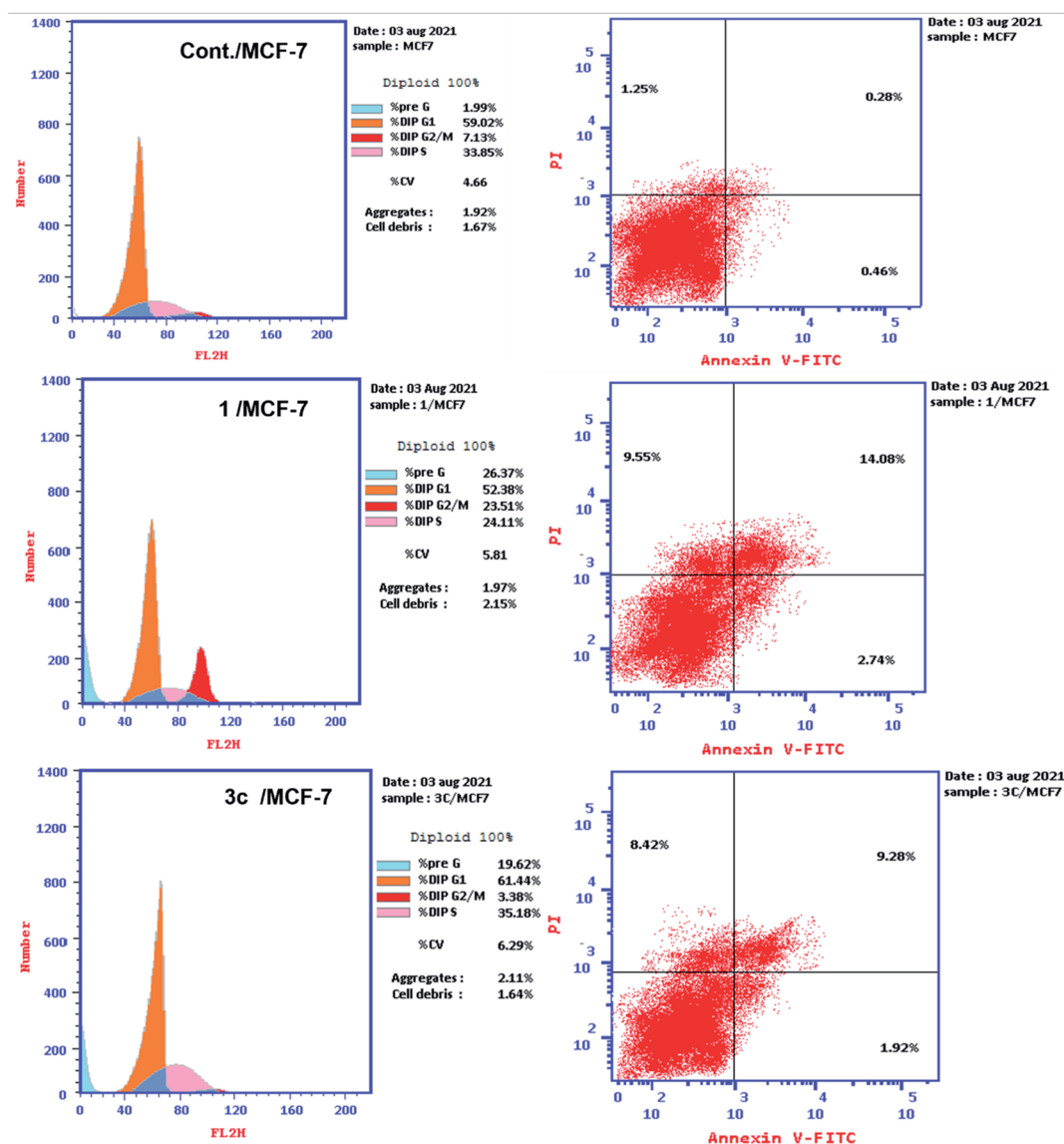


Fig. 4 Cell cycle analysis of and activation of apoptosis caused by the derivatives **1** and **3c** against MCF-7 cells.



their inhibitory activities against EGFR, VEGFR-2 and BRAF^{V600E}.^{61–63} More details in the ESI.†

2.2.3. *In vitro* DNA-flow cytometric (cell cycle) analysis. To determine the distribution of cell lines in each phase of cell cycle, the PI was used to stain the DNA content of each cell line. At a density of 1×10^6 to 3×10^6 cells per dish, MCF-7 cells were seeded in 30 mm tissue culture plates in 5 mL of complete medium.⁶³ More details in the ESI.†

2.2.4. Annexin V-FITC apoptosis assay. Annexin V-FITC apoptosis detection kit (BD biosciences) was used to quantify the percentage of cells undergoing apoptosis and to determine the mode of cell death whether by apoptosis or necrosis in the presence or absence of the active compounds **1**, **3c**. The experiment was carried out according to the manufacturer's protocol.⁶³ More details in the ESI.†

2.2.5. Antimicrobial activity assay. *In vitro* microbial activities were carried out at the Regional Center for Mycology and Biotechnology (RCMB), Al-Azhar University, Cairo, Egypt. The biological potential of the newly prepared target structures was inspected toward the examined organisms and expressed as the diameter of the inhibition zones due to the agar plate diffusion technique.^{64–69} More details in the ESI.†

2.2.5.1. Minimal inhibitory concentration (MIC) measurement. The bacteriostatic activity of the compounds was then evaluated using the two-fold serial dilution technique. Two-fold serial dilutions of the tested compounds solutions were prepared using the proper nutrient broth.^{67–69} More details in the ESI.†

2.3. Computational studies

2.3.1. Molecular docking. The 2D structure of the newly synthesized derivatives **1** and **3c** was drawn through ChemDraw. The protonated 3D was employed using standard bond lengths and angles, using Molecular Operating Environment (MOE-Dock) software version 2014.0901.^{70–72} Then, the geometry optimization and energy minimization were applied to get the Conf Search module in MOE, followed by saving of the MOE file for upcoming docking process. The co-crystallized structures of EGFR, VEGFR-2 and BRAF^{V600E} kinases with their ligands erlotinib, sorafenib and SB-590885 were downloaded (PDB codes: 1M17, 4ASD and 2FB8, respectively) from protein data bank.^{73–75} More details in the ESI.†

2.3.2. *In silico* toxicity potential. Toxicity risks and physicochemical characteristics were given for the newly synthesized derivatives following Osiris methodology and mentioned in details within the ESI.†⁷⁶

3. Results and discussion

3.1. Chemistry

An efficient synthesis of the new thienothiazoles **3a–d** and thiazolothiazoles **5a–d** has been performed starting with (1,5-dimethyl-3-oxo-2-phenyl-2,3-dihydro-1H-pyrazol-4-yl)carbamic chloride.⁵⁹ Their synthetic routes were outlined in (Schemes 1 and 2). Refluxing 2-chloro-*N*-(1,5-dimethyl-3-oxo-2-phenyl-2,3-dihydro-1H-pyrazol-4-yl)acetamide with ammonium

thiocyanate in ethanol produced the corresponding thiazolidin-4-one derivative **1**. The ¹H-NMR spectrum of compound **1** appeared three singlet signals at δ 2.15, 3.21 and 4.06 ppm due to CH₃, NCH₃ and CH₂ respectively and also, its ¹³C-NMR spectrum showed signals at δ 12.11, 32.04 and 35.16 ppm due to CH₃, NCH₃ and CH₂ respectively.

The Gewald reaction is a condensation of ketone or aldehyde with acetonitriles substituted by a strong electron withdrawing group (such as ester, amide, and nitrile) in the presence of elemental sulfur and base to give a poly-substituted 2-aminothiophene. So, the thieno[3,2-*d*]thiazole derivatives **3a–d** were obtained *via* the treatment of key compound **1** according to Gewald reaction with a series of active methylene derivatives namely; malononitrile, ethyl cyanoacetate, cyanoacetohydrazide and/or cyanothioacetamide in the presence of sulfur and triethylamine. IR spectrum of the compound **3a** showed bands at 3415, 3373 cm^{−1} referring to NH₂ and strong absorption band at 2212 cm^{−1} due to CN. The ¹H-NMR spectrum of compound **3b** displayed triplet and quartet signals at δ 1.23 and 4.15 ppm according to the ester group (Scheme 1).

Furthermore, reaction of thiazolidin-4-one moiety **1** with different isothiocyanate derivatives namely; phenyl isothiocyanate, ethyl isothiocyanate, methyl isothiocyanate and/or *p*-chloro phenyl isothiocyanate in the presence of sulfur and triethylamine afforded the corresponding dihydrothiazolo[4,5-*d*]thiazole derivatives **5a–d** respectively. The ¹H-NMR spectrum of compound **5b** displayed triplet and quartet signals at δ 1.22 and 4.15 ppm according to the ethyl group and its ¹³C-NMR showed signals at δ 13.92, 51.20 and 184.27 ppm referring to ethyl and C=S groups (Scheme 2).

3.2. Biological activity

3.2.1. *In vitro* anti-proliferative activity. The cytotoxic activity of the newly synthesized compounds was assessed against two cancer cell lines; human breast adenocarcinoma (MCF-7) and hepatocellular carcinoma (HepG-2) using MTT assay.⁶⁰ These types of cancer cell lines have a high expression of EGFR, VEGFR and BRAF.^{10,11,17,18,26} In addition, the cytotoxic effect of the new compounds was also evaluated against the

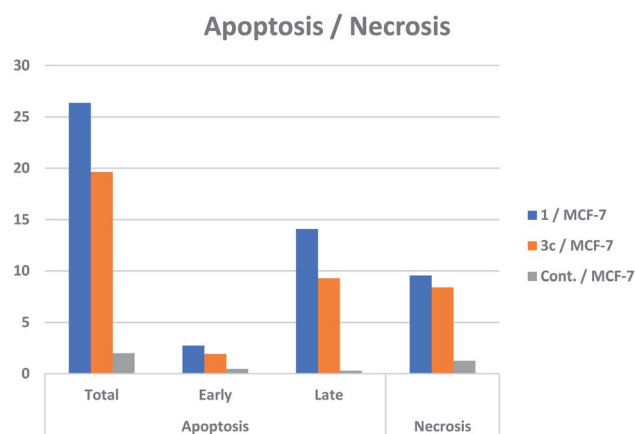


Fig. 5 Apoptosis induction induced by the derivatives **1**, **3c**.



normal lung fibroblast (WI38) to demonstrate their safety profiles. The commercially available doxorubicin was utilized as a standard drug. The resultant data represented the concentrations of the derivatives that led to 50% inhibition of cell viability (IC_{50} , μM) which were reported in Table 1. According to IC_{50} values in Table 1 it has been revealed that the evaluated compounds exhibited versatile anti-proliferative activities against the cell lines under study. Interestingly, the starting pyrazolinyl-aminothiazol-4-one **1** produced the most significant cytotoxic activity. It evidently reduced the viability of both MCF-7 and HepG-2 in an equipotent manner to that of doxorubicin with IC_{50} values of 4.02 ± 0.02 , 4.52 ± 0.04 μM , respectively, IC_{50} doxorubicin; 4.62 ± 0.0 , 5.66 ± 0.01 μM , respectively. A mild decrease in the activity against both cancer cell lines (about 1.8 and 1.3 folds, respectively) was detected by the thieno[3,2-*d*]thiazole-carbohydrazide derivative **3c** of IC_{50} values; 8.35 ± 0.03 and 7.88 ± 0.01 μM , respectively. The carbohydrazide side

chain produced an important point for hydrogen binding interaction with the target proteins. On the other hand, the rest of compounds showed moderate to weak cytotoxic activities. This result indicated that the conjugation of the thiazolinone moiety with the pyrazolinone nucleus produced a significant cytotoxic potency, while the fused thieno[3,2-*d*]thiazole or dihydrothiazolo[4,5-*d*]thiazole scaffolds negatively affect the activity, which might be due to improper fitting in the active sites of the proteins which they act on.

The safety of the most active compounds **1**, **3c** towards the normal fibroblasts (WI-38) cell line was also examined. The tested compounds were found to be more selective to MCF-7 and HepG-2 cancer cell lines than to the normal cell line WI-38 as they revealed cytotoxicity with IC_{50} of 60.44, 54.72 μM . Therefore, they can be considered to be safe candidates against the normal cell line.

Table 3 *In vitro* antimicrobial activities of the synthesized compounds using well diffusion agar assay and expressed as mean diameter of inhibition zones (mm)

Mean diameter of inhibition zone (mean \pm SEM) (mm)								
Cpd. no.	Gram +ve bacteria			Gram –ve bacteria			Fungi	
	<i>S. aureus</i> 25923	<i>E. faecalis</i>	<i>S. pneumoniae</i> 010010	<i>E. coli</i> RCMB 010052	<i>S. typhi</i> ATCC 14028	<i>P. aeruginosa</i>	<i>A. fumigatus</i> RCMB 02568	<i>C. albicans</i> ATCC 10231
1	31 \pm 0.17	28 \pm 0.92	30 \pm 0.87	26 \pm 0.22	21 \pm 0.54	27 \pm 0.51	25 \pm 0.88	22 \pm 0.30
3a	28 \pm 0.15	13 \pm 0.76	21 \pm 0.69	25 \pm 0.15	17 \pm 0.95	22 \pm 0.44	18 \pm 0.25	12 \pm 0.51
3b	19 \pm 0.68	20 \pm 0.24	14 \pm 0.84	15 \pm 0.71	23 \pm 0.79	17 \pm 0.41	21 \pm 0.22	11 \pm 0.70
3c	30 \pm 0.47	27 \pm 0.36	25 \pm 0.17	28 \pm 0.92	21 \pm 0.16	23 \pm 0.13	24 \pm 0.15	18 \pm 0.67
3d	13 \pm 0.95	22 \pm 0.11	28 \pm 0.45	22 \pm 0.14	18 \pm 0.13	20 \pm 0.19	19 \pm 0.45	16 \pm 0.28
5a	21.2 \pm 0.25	13 \pm 0.43	NA	NA	23 \pm 0.05	NA	9 \pm 0.53	NA
5b	16 \pm 0.88	27 \pm 0.41	28 \pm 0.12	10 \pm 0.42	NA	18 \pm 0.95	NA	12 \pm 0.07
5c	20 \pm 0.08	24 \pm 0.89	15 \pm 0.86	25 \pm 0.10	17 \pm 0.78	22 \pm 0.48	26 \pm 0.17	19 \pm 0.23
5d	25 \pm 0.13	NA	NA	15 \pm 0.04	NA	13 \pm 0.11	NA	NA
^a S	26 \pm 0.45	25 \pm 0.38	22 \pm 0.81	27 \pm 0.56	23 \pm 0.92	20 \pm 0.53	—	—
^a A	—	—	—	—	—	—	22 \pm 0.72	20 \pm 0.78

^a Streptomycin and Amphotericin B were used as standard drugs against the tested bacteria and fungi, respectively.

Table 4 Minimal inhibitory concentrations (MIC) (μM) of the target compounds against the tested pathogenic bacteria and fungi

Cpd. no.	Gram +ve bacteria			Gram –ve bacteria			Fungi	
	<i>S. aureus</i> 25923	<i>E. faecalis</i>	<i>S. pneumoniae</i> 010010	<i>E. coli</i> RCMB 010052	<i>S. typhi</i> ATCC 14028	<i>P. aeruginosa</i>	<i>A. fumigatus</i> RCMB 02568	<i>C. albicans</i> ATCC 10231
1	3.63	16.14	3.94	18.33	62.18	7.52	20.81	38.26
3a	16.85	185.18	58.86	19.36	125.14	40.45	120.05	186.11
3b	78.98	67.41	178.52	118.98	45.62	124.84	62.12	189.05
3c	4.12	17.28	20.15	14.18	64.05	42.18	19.23	18.41
3d	181.12	75.47	16.18	71.82	121.43	67.02	117.96	132.26
5a	63.57	183.27	—	—	44.68	—	197.41	—
5b	135.36	15.18	15.87	193.20	—	121.75	—	185.13
5c	68.75	18.86	178.06	20.75	125.36	62.25	17.83	79.42
5d	18.87	—	—	118.15	—	180.25	—	—
^a aS	16.75	19.48	65.33	9.18	47.12	68.25	—	—
^a aA	—	—	—	—	—	—	39.15	67.82

^a Streptomycin and amphotericin B were used as standard drugs against the tested bacteria and fungi, respectively.



3.2.2. The inhibitory effect of compounds 1, 3c towards EGFR, VEGFR-2 and BRAF^{V600E} tyrosine kinases. The most active cytotoxic agents 1, 3c were also evaluated as multitargeted protein kinases against EGFR, VEGFR-2 and BRAF^{V600E} tyrosine kinases and sorafenib was used as a positive control.^{61,62} The obtained results were summarized in Table 2. A significant sensitivity was detected by EGFR kinase against both compounds 1, 3c which revealed a near equipotent or slightly higher inhibitory activity than that of the reference drug sorafenib with IC₅₀ s; 0.022, 0.017 μ M, respectively, while IC₅₀

sorafenib; 0.025 μ M. On the other hand, about 2.4–2.2 folds decrease in the inhibitory activity was detected by the tested derivatives 1, 3c against the target VEGFR-2 while of IC₅₀ s; 2.470, 2.259 μ M, respectively comparing to sorafenib with IC₅₀; 1.022 μ M. Furthermore, the thieno[3,2-*d*]thiazole derivative 3c exhibited a promising inhibitory activity against BRAF^{V600E} but slightly less than that of standard drug sorafenib with IC₅₀ s; 0.088, 0.040 μ M, respectively. On the other hand, a remarkable drop in the activity was detected by the pyrazoliny-thiazolinone derivative 1 against BRAF^{V600E} employing IC₅₀; 2.026 μ M. It

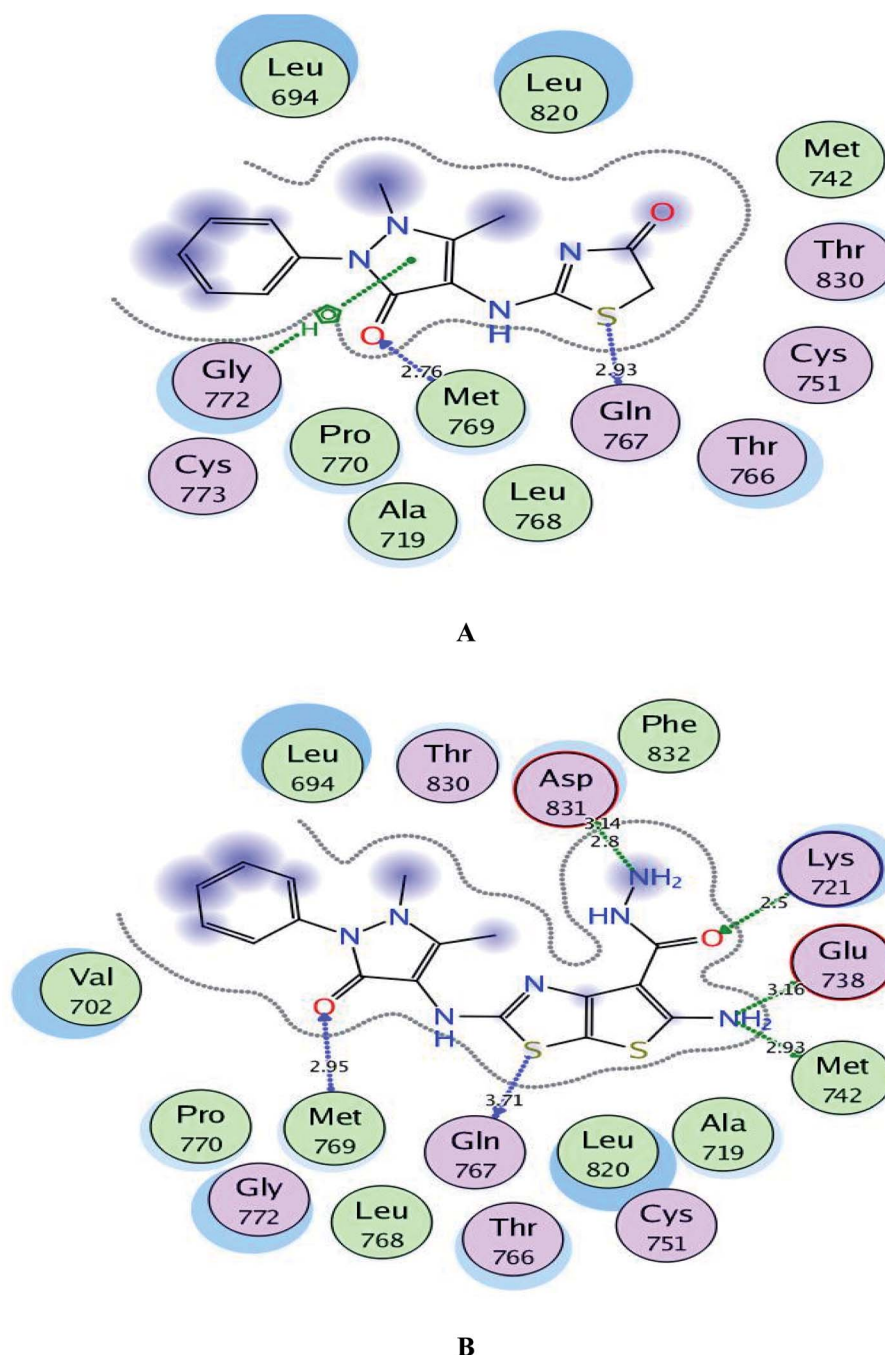


Fig. 6 A and B maps illustrate the 2D binding features of the promising targets 1 and 3c within the active site of EGFR (PDB code: 1M17), respectively.



could be noticed that the bicyclic thieno-thiazole pharmacophore produced a positive impact towards the inhibition effect against target BRAF^{V600E} kinase.

3.2.3. *In vitro* DNA-flow cytometric (cell cycle) analysis. The most potent analogues **1**, **3c** were selected to study their effects on cell cycle progression in MCF-7 cell line. DMSO was utilized as a negative control. The stages of cell cycle were being detected *via* flow cytometry after propidium iodide (PI) staining followed by RNase treatment.⁶³ In this experiment, MCF-7 cells

were incubated with a concentration of 4.021 μ M for compound **1** and with 8.35 μ M for compound **3c** for 24 h. The flow cytometry approach was used to quantify cell populations at various stages of the cell cycle (pre-G1, G1, S and G2/M phases). The obtained results indicated that MCF-7 cells treatment with compounds **1** and **3c** led to an interference with the normal cell cycle distribution. The compound **1** produced a remarkable increase in the percentages of the cells at pre-G1 and G2/M phases from 1.99% and 7.31%, respectively in the control

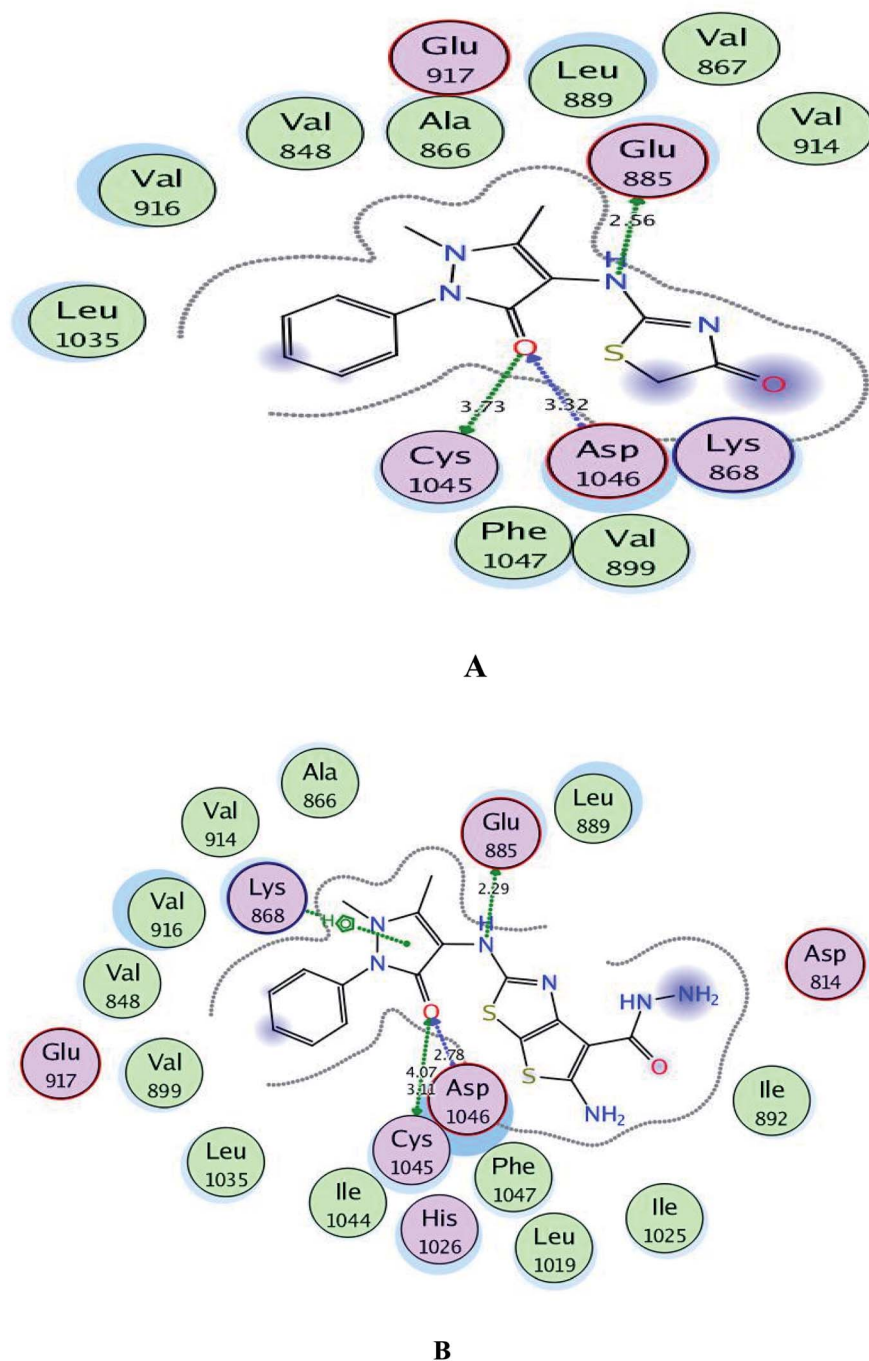


Fig. 7 A and B maps illustrate the 2D binding features of the promising targets, **1** and **3c** within the active site of VEGFR-2 (PDB code: 4ASD), respectively.

cells to reach to 26.37% and 23.51% in MCF-7 cells treated with compound **1**. Such increase was accompanied by an observable reduction in the percentages of cells at G1 and S-stages of the cell cycle from 59.02% and 33.85% in the control cells to 52.38% and 24.11% in the treated cells. This result clearly investigated that compound **1** arrested the cell cycle at G2/M phase. On the other hand, compound **3c** induced an increase in the percentages of cells at pre-G1 and S-phases to reach to 19.62% and 35.18% comparing to the control cells and decreased cell

percentage at G2/M phase from 33.85% in control cells to 3.38% in the treated cells. This result represented that there was cell cycle arrest at S phase and cessation of mitotic cycle (Fig. 4).

3.2.4. Determination of apoptosis using annexin V-FITC staining technique. The apoptotic mode of cell death induced by compounds **1** and **3c** was further determined to find out whether the cell death was due to apoptosis or necrosis. This assay was carried out using annexin V/PI assay. Annexin V conjugated with FITC was utilized to stain cells in combination

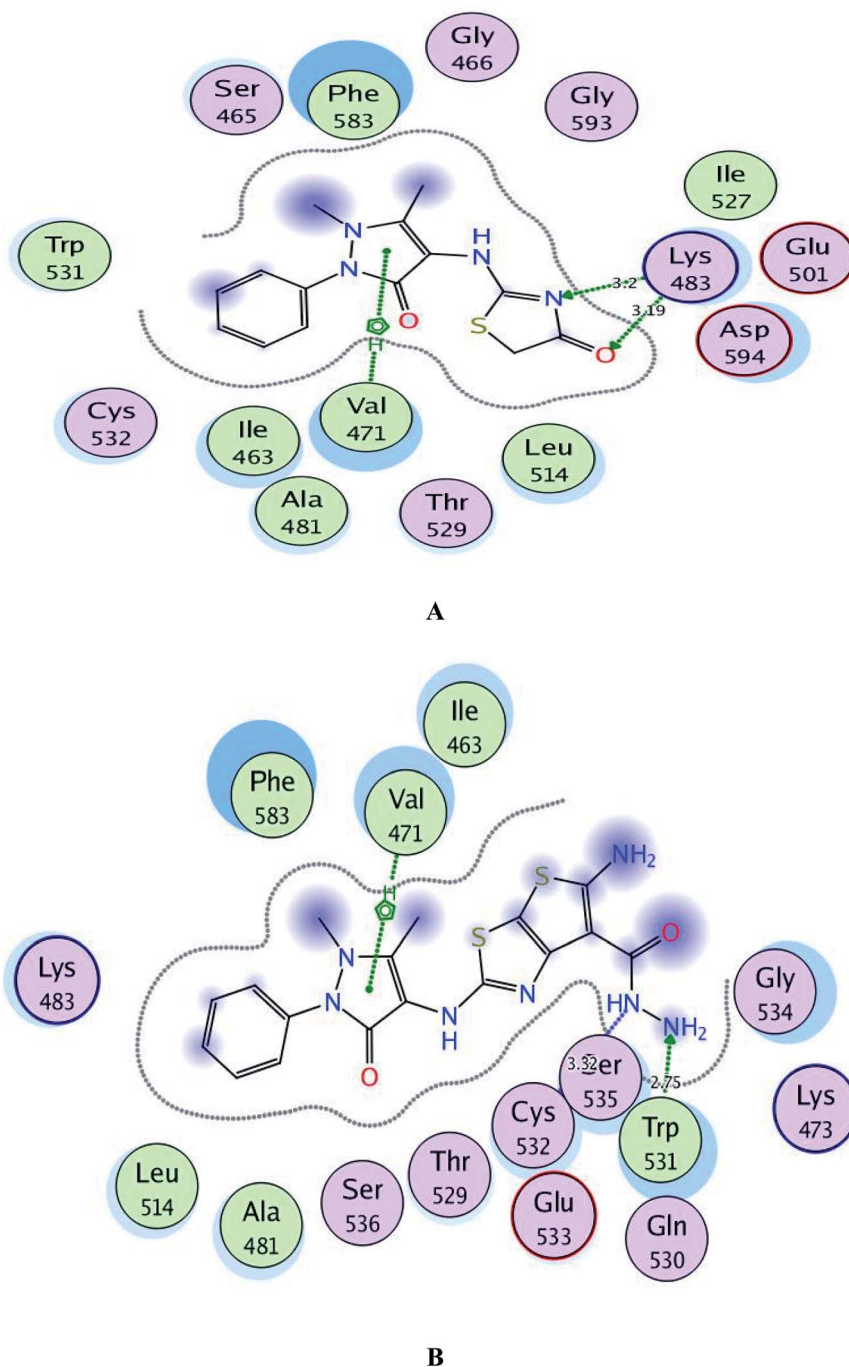


Fig. 8 A and B maps illustrate the 2D binding features of the promising targets, **1** and **3c** within the active site of BRAF^{V600E} (PDB code: 2FB8), respectively.



with PI.⁶³ The cells which stained positive for annexin V/PI indicated the cells in the late apoptotic stage which have lost the integrity of their membranes.⁶³ MCF-7 cells were treated with the tested derivatives **1** and **3c** at their IC₅₀ concentrations 4.021 μM and 8.35 μM , respectively for a period of 24 h. Then staining of MCF-7 cells was carried out using two dyes; annexin V/propidium iodide (PI). Flow cytometry technique has detected the corresponding red (PI) and green (FITC) fluorescence. The representative dot plots of flow cytometric analyses exhibited four various distributions (Fig. 4): lower left (annexin V and PI negative) represents the healthy cells, lower right (annexin V positive and PI negative) represents the cells in early apoptosis, upper right (annexin V and PI positive) represents cells in late apoptosis and finally upper left (annexin V negative and PI positive) dead or necrotic cells. Both compounds have increased the early apoptosis from 0.47% (DMSO control) to 2.74% and 1.92%, respectively. Also, there was an increase in the late apoptosis by both **1** and **3c** from 0.28% (DMSO control) to 14.08% and 9.28%, respectively with necrotic percent of 9.55% and 8.42% vs. 0.66% produced by DMSO control. It was observable that the late apoptosis percentage caused by compounds **1**, **3c** was higher than that of the early phase making it more challenging to recover the apoptotic cells to the safe ones. The obtained results investigated that apoptosis was one of the main mechanisms of compounds **1**, **3c** to inhibit cancer cell proliferation (Fig. 5).

3.2.5. Antimicrobial activity. It has been employed that various pyrazole and thiazole motifs constitute the main blocks in various promising antimicrobial compounds.^{64,65} Thus, it was interest to assess the antimicrobial activity of the newly prepared compounds alongside their cytotoxic evaluation as an effort to gain new candidates of dual potent anticancer and antimicrobial activities. The antimicrobial potency of the new compounds **1–5** was *in vitro* screened versus a panel of pathogenic microbes: Gram-positive bacteria viz. *S. aureus*, *E. faecalis*, Gram-negative bacteria viz. *S. pneumoniae*, *E. coli*, *S. typhi* and two fungal and yeast strains viz. *A. fumigatus*, *C. albicans* using streptomycin and amphotericin B as reference drugs for antibacterial and antifungal activity, respectively. Agar well diffusion approach was used to examine the antimicrobial activity of all synthesized compounds and the obtained data for each examined compound were recorded as the mean diameter of inhibition zones (mm) for the bacterial or fungal growth around the discs⁶⁷ (Table 3). Moreover, two-fold serial dilution approach was used to find out the Minimum Inhibitory Concentration (MIC) values (expressed in $\mu\text{g mL}^{-1}$) for the examined compounds.^{68,69} The obtained data were recorded in (Table 4).

Based on the MIC records in Table 4, it has been detected that there is a wide variability in the antimicrobial potency of the newly tested members. Evidently, the pyrazolinyl-aminothiazol-one **1** and the thieno[3,2-*d*]thiazole-carbohydrazide derivative **3c** produced the most potent broad spectrum antimicrobial activity against the test bacterial and fungal strains.

It has been detected that the compounds **1** and **3c** exhibited selective antibacterial activity against the tested Gram-positive bacteria of 1.20–16 folds more potency than streptomycin of

MIC range; 3.63–20.15 μM , MIC_{streptomycin}; 16.75–65.33 μM . Conversely, the potency of the latter compounds decreased by 2 and 1.3 folds against the Gram-negative bacteria *S. pneumoniae* and *E. coli* of MIC range; 14.18–64.05 μM , MIC_{streptomycin}; 9.18, 47.12 μM . On the other hand, *P. aeruginosa* strain represented greater selectivity towards **1**, **3c** than streptomycin of MIC values; 7.52, 42.18 μM , respectively, MIC_{streptomycin}; 68.25 μM . In addition, the fungal and yeast strains under study exhibited 1.8–3.6 times more sensitivity towards the compounds **1** and **3c**

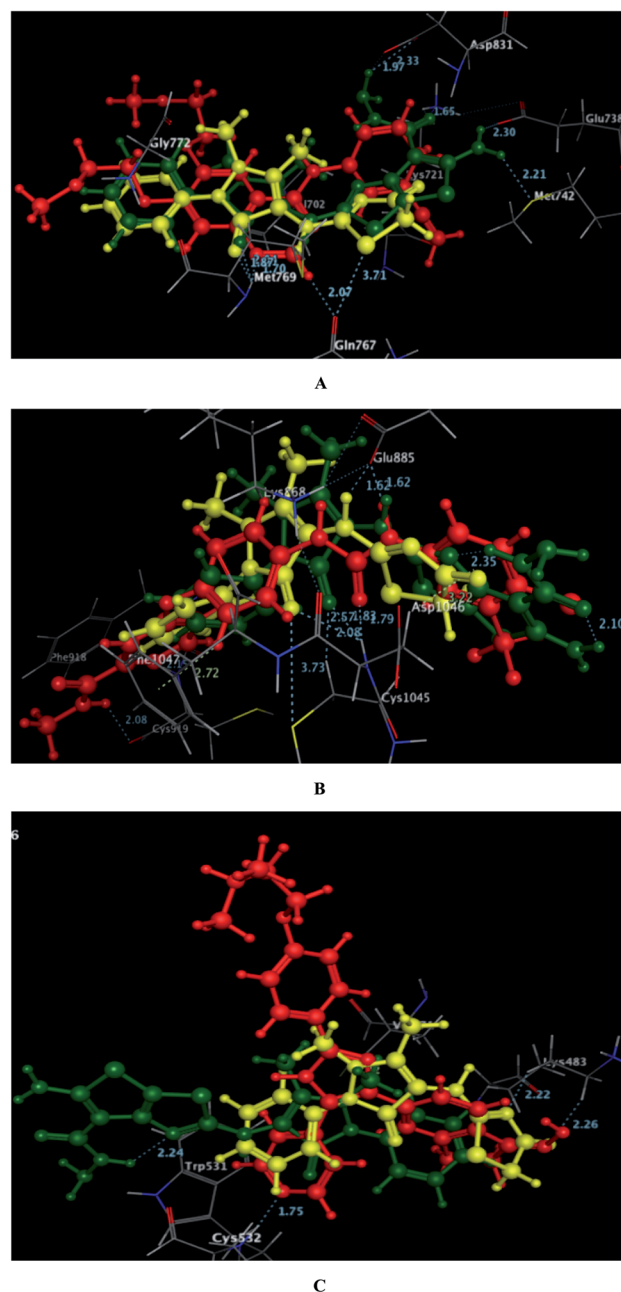


Fig. 9 A–C diagrams explore the 3D superimposition between the promising targets, **1** (yellow), **3c** (green) and the docked original ligands, erlotinib, sorafenib and SB-590885 (red) within the binding sites of EGFR, VEGFR-2 and BRAF^{V600E} (PDB codes: 1M17, 4ASD and 2FB8, respectively).



Table 5 Predictive toxicity of the synthesized compounds according to molinspiration software

Comp. no.	Toxicity risks				Solubility	Drug-likeness	Drug score
	Mutagenicity	Tumorigenicity	Irritancy	Reproductive effect			
1	Red	Red	Green	Green	−2.62	5.3	0.33
3a	Red	Red	Green	Green	−5.83	0.88	0.18
3b	Red	Red	Green	Green	−5.5	1.85	0.19
3c	Red	Red	Green	Green	−5.43	0.05	0.16
3d	Red	Red	Green	Green	−5.08	5.14	0.23
5a	Red	Red	Green	Green	−6.94	5.38	0.16
5b	Red	Red	Green	Green	−5.22	5.8	0.23
5c	Red	Red	Green	Green	−4.92	5.19	0.24
5d	Red	Red	Green	Green	−7.68	5.83	0.14

than the reference drug amphotericin B producing MIC range 18.41–38.26 μM , MIC_{amphotericin B}; 68.25 μM . Furthermore, the thieno [3,2-*d*]thiazole-6-carbonitrile analogue **3a** produced equipotent antibacterial activity to streptomycin against *S. aureus* and 1.1, 1.6 folds more potency against *S. pneumoniae* and *P. aeruginosa* of MIC values; 16.85, 58.86 μM . On the other hand, the antifungal activity **3a** was completely lost against the tested fungal and yeast strains. Overall, a majority of the target compounds showed moderate to weak activity against the tested kinds of susceptible strains.

The obtained results confirmed that the compounds **1** and **3c** among the whole tested derivatives were the most promising antimicrobial agents against the examined Gram-positive bacteria and the fungal strains, but they produced a slightly weaker activity against the examined Gram-negative microbes.

3.3. Computational studies

3.3.1. Molecular docking study on EGFR, VEGFR-2 and BRAF^{V600E}. The docking simulation was applied in attempt to achieve further vision of the binding modes and orientations of the promising derivatives **1** and **3c** into the binding sites of EGFR, VEGFR-2 and BRAF^{V600E} kinases. This study was done using MOE-Dock (Molecular Operating Environment) software version 2014.0901.^{70–72} The docking process was first validated through self-docking of the co-crystallized ligands erlotinib, sorafenib and SB-590885 within the active sites of EGFR, VEGFR-2 and BRAF^{V600E} (PDB codes: 1M17, 4ASD and 2FB8, respectively)^{73–75} giving energy scores of −12.23, −11.50 and −11.37 kcal mol^{−1} with small RMSD values of 0.88, 1.24 and 1.35 Å, respectively between the co-crystallized ligands and their docked poses.

As depicted in Fig. 6, the targets **1** and **3c** were bound to the active site of EGFR with energy scores of −11.67 and −11.83 kcal mol^{−1}, respectively through formation of two H-bonds, one acceptor between the oxygen of the pyrazolone moiety and the backbone of the key amino acid Met769, and the other one was donor between the thiazolyl sulfur and the backbone of Gln767 (distance: 2.76 & 2.93 Å in compound **1** and 2.95 & 3.71 Å in compound **3c**, respectively). Also, the pyrazolone centroid of compound **1** afforded arene-cation interaction with Gln772. On the other hand, the nitrogen of the

amino group at p-2 of thienothiazole moiety in compound **3c** gave two H-bond donors with the sidechains of Glu738 and Met742 (distance: 3.16 and 2.93 Å, respectively). Also, the carbonyl fragment improved fixation of compound **3c** through formation of additional H-bonds. One was between the oxygen and the sidechain of Lys721 (distance: 2.50 Å, respectively), and the two others were between the amino nitrogen and the sidechain of Asp831 (distance: 2.80 and 3.14 Å, respectively).

Regarding to binding to VEGFR-2 active site in Fig. 7, it was observed that the pyrazolinone oxygen and NH linker in both compounds played an essential role in the fixation through formation of hydrogen bonding with the amino acids Cys1045, Asp1046 and Glu885. Moreover, the pyrazolinone scaffold in compound **3c** displayed arene-cation interaction with Lys868. The targets **1** and **3c** provided small energy scores of −10.63 and −11.22 kcal mol^{−1}, respectively confirming their stability within the binding pocket.

By inspection of Fig. 8, the derivatives **1** and **3c** were bound to the vicinity of BRAF^{V600E} with energy scores of −10.25 and −10.92 kcal mol^{−1}, respectively through arene-cation interaction between the pyrazolinone moiety and the amino acid Val471. Furthermore, the nitrogen and the carbonyl oxygen of thiazolinone scaffold in compound **1** exhibited two H-bond acceptors with the sidechain of Lys483 (distance: 3.20 and 3.19 Å, respectively). While the two nitrogens of the hydrazide fragment in the compound **3c** revealed two H-bonds with the sidechain of Trp531 and the backbone of Cys532 (distance: 2.75 and 3.32 Å, respectively).

Finally and regarding to the superimposition Fig. 9, it was noted that the presence of pyrazolinone scaffold linked to thiazolinone moiety in compound **1** or thieno[3,2-*d*]thiazole-6-carbohydrazide in compound **3c** gave the chance for good fitting within the active sites of EGFR, VEGFR-2 and BRAF^{V600E} with a relatively similar binding behavior as the original ligands erlotinib, sorafenib and SB-590885 through arene-cation and H-bond interactions.

3.3.2. In silico toxicity potential. The newly synthesized analogues were estimated for toxicity risks and physicochemical characteristics *via* Osiris methodology.⁷⁶ The toxicity parameters including mutagenicity, tumorigenicity, skin irritancy and reproductive effect were predicted for all compounds **1–5** and



the results were cited in Table 5. The resultant data showed that all the compounds would be safe and were predicted to have no side effects. Drug score measures the compound's potential to have drug-conform behavior. Accordingly, the highest drug-score value was obtained by compound **1** proving its both effectiveness and potentiality as a new drug member.

4. Conclusions

This context represents the design and synthesis of two sets of derivatives bearing pyrazoline-3-one ring integrated either with the thieno[3,2-*d*]thiazole or with thiazolo[4,5-*d*]thiazolidine-2-thione scaffolds *via* NH linker, **3a-d**, **5a-d**, respectively using the pyrazolinyl-thiazolinone derivative **1** as a key precursor. All the new derivatives were evaluated as cytotoxic candidates against two human cancer cell lines; breast MCF-7 and hepatocellular HepG-2, using doxorubicin as a reference drug. Compounds **1** and **3c** revealed significant inhibitory activities against both cancer cell lines with IC₅₀s ranging from 4.02–8.35 μM, comparing to doxorubicin of IC₅₀s; 4.62, 5.66 μM. In addition, compounds **1** and **3c** showed a promising safety profile against the normal WI38 cell line. Furthermore, the compounds were evaluated as multitargeting protein kinase inhibitors against EGFR, VEGFR-2 and BRAF^{V600E}. Both compounds showed the most potent suppression effect against EGFR of IC₅₀s; 0.022, 0.017 μM, comparing to the reference drug sorafenib of IC₅₀; 0.025 μM. The inhibitory activities of **1** and **3c** decreased slightly against VEGFR-2 and BRAF^{V600E} of IC₅₀ range; 0.040–2.259 μM, IC₅₀ sorafenib; 1.022, 0.040 μM. Moreover, compounds **1** and **3c** were tested for their impact on cell cycle progression and induction of apoptosis in the MCF-7 cell line. It was investigated that they produce an apoptotic effect and cell cycle arrest. Additionally, all the new analogues were assessed as antibacterial and antifungal agents against a number of pathogenic Gram-positive, Gram-negative bacteria, yeast and fungi in comparison to streptomycin and amphotericin-B. Interestingly, both **1** and **3c** appeared the most potent antimicrobial members against the examined microbial stains considering both compounds having dual anticancer and antimicrobial activities. Molecular docking study rationalized the promising suppression effect of **1** and **3c** against EGFR, VEGFR-2 and BRAF^{V600E} due to their good fitting and the binding energy scores in the active site of the tested kinases. Additional toxicity study was performed for all new derivatives which represented their good drug-likeness properties and medium toxicity risks in humans.

Conflicts of interest

The authors declare that they have no conflict of interest.

Acknowledgements

The authors are thankful to the Faculty of Pharmacy-Al-Azhar University/Egypt, for performing the spectral and biological data of the new target compounds.

References

- 1 J. Ferlay, M. Laversanne, M. Ervik, F. Lam, M. Colombet, L. Mery, M. Piñeros, A. Znaor, I. Soerjomataram and F. Bray, *Global Cancer Observatory: Cancer Tomorrow*, Lyon, France, International Agency for Research on Cancer, 2020, <https://gco.iarc.fr/tomorrow>.
- 2 S. O. Zariaei, R. M. Sbenati, N. N. Alach, H. S. Anbar, R. El-Gamal, H. Tarazi, M. K. Shehata, M. S. Abdel-Maksoud, C.-H. Oh and M. I. El-Gamal, *Eur. J. Med. Chem.*, 2021, **224**, 113674.
- 3 R. Awasthi, A. Roseblade, P. M. Hansbro, M. J. Rathbone, K. Dua and M. Bebawy, *Curr. Drug Targets*, 2018, **19**, 1696–1709.
- 4 Z. Du and C. M. Lovly, *Mol. Cancer*, 2018, **17**, 58.
- 5 N. Iqbal and N. Iqbal, *Chemother. Res. Pract.*, 2014, **2014**, 357027.
- 6 B. J. Druker, *Trends Mol. Med.*, 2002, **8**, S14–S18.
- 7 K. S. Bhullar, N. O. Lagarón, E. M. McGowan, I. Parmar, A. Jha, B. P. Hubbard and H. V. Rupasinghe, *Mol. Cancer*, 2018, **17**, 1–20.
- 8 H. Kittler and P. Tschandl, *Br. J. Dermatol.*, 2018, **178**, 26–27.
- 9 A. Ayati, S. Moghimi, S. Salarinejad, M. Safavi, B. Pouramiri and A. Foroumadi, *Bioorg. Chem.*, 2020, **99**, 103811.
- 10 R. R. Khattab, A. A. Hassan, D. A. A. Osman, F. M. Abdel-Megeid, H. M. Awad, E. S. Nossier and W. A. El-Sayed, *Nucleosides, Nucleotides Nucleic Acids*, 2021, **40**, 1090–1113.
- 11 F. Ciardiello and G. Tortora, *Clin. Cancer Res.*, 2001, **7**, 2958–2970.
- 12 R. R. Khattab, A. K. Alshamari, A. A. Hassan, H. H. Elganzory, W. A. El-Sayed, H. M. Awad, E. S. Nossier and N. A. Hassan, *J. Enzyme Inhib. Med. Chem.*, 2021, **36**, 504–516.
- 13 I. M. Othman, Z. M. Alamshany, N. Y. Tashkandi, M. A. Gad-Elkareem, M. M. Anwar and E. S. Nossier, *Bioorg. Chem.*, 2021, **114**, 105078.
- 14 P. Carmeliet, *Oncology*, 2005, **69**, 4–10.
- 15 D. J. Hicklin and L. M. Ellis, *J. Clin. Oncol.*, 2005, **23**, 1011–1027.
- 16 Z. K. Otroek, J. A. Makarem and A. I. Shamseddine, *Blood Cells, Mol., Dis.*, 2007, **38**, 258–268.
- 17 A. S. Oguntade, F. Al-Amodi, A. Alrumayh, M. Alobaida and M. Bwalya, *J. Egypt. Natl. Cancer Inst.*, 2021, **33**, 1–11.
- 18 D. H. Dawood, E. S. Nossier, M. M. Ali and A. E. Mahmoud, *Bioorg. Chem.*, 2020, **101**, 103916.
- 19 W. S. El-serwy, H. S. Mohamed, W. S. El-serwy, N. A. Mohamed, E. M. Kassem, K. Mahmoud and E. S. Nossier, *ChemistrySelect*, 2020, **5**, 15243–15253.
- 20 L. Zhong, Y. Li, L. Xiong, W. Wang, M. Wu, T. Yuan, W. Yang, C. Tian, Z. Miao, T. Wang and S. Yang, *Signal Transduction Targeted Ther.*, 2021, **6**, 201.
- 21 F. Wang, J. Molina, D. Satele, J. Yin, V. S. Lim and A. A. Adjei, *Invest. New Drugs*, 2019, **37**, 658–665.
- 22 M. Y. Zhao, Y. Yin, X. W. Yu, C. B. Sangani, S. F. Wang, A. M. Lu, L. F. Yang, P. C. Lv, M. G. Jiang and H. L. Zhu, *Bioorg. Med. Chem.*, 2015, **23**, 46–54.

- 23 T. I. Bonner, S. B. Kerby, P. Suttrave, M. A. Gunnell, G. Mark and U. R. Rapp, *Mol. Cell. Biol.*, 1985, **5**, 1400–1407.
- 24 T. Bonner, S. J. O'Brien, W. G. Nash, U. R. Rapp, C. C. Morton and P. Leder, *Science*, 1984, **223**, 71–74.
- 25 P. C. Sharma, K. K. Bansal, A. Sharma, D. Sharma and A. Deep, *Eur. J. Med. Chem.*, 2020, **188**, 112016.
- 26 M. S. Abdel-Maksoud, M. I. El-Gamal, B. S. Lee, M. M. Gamal El-Din, H. R. Jeon, D. Kwon, U. M. Ammar, K. I. Mersal, E. M. Ali, K. T. Lee and K. H. Yoo, *J. Med. Chem.*, 2021, **64**, 6877–6901.
- 27 R. Bansal and A. Malhotra, *Eur. J. Med. Chem.*, 2020, **12**, 113016.
- 28 A. R. Sayed, S. M. Gomha, F. M. Abdelrazek, M. S. Farghaly, S. A. Hassan and P. Metz, *BMC Chem.*, 2019, **13**, 1–3.
- 29 X. Deng, X. Tan, T. An, Q. Ma, Z. Jin, C. Wang, Q. Meng and C. Hu, *Molecules*, 2019, **24**, 682.
- 30 H. K. Mahmoud, T. A. Farghaly, H. G. Abdulwahab, N. T. Al-Qurashi and M. R. Shaaban, *Eur. J. Med. Chem.*, 2020, **208**, 112752.
- 31 C. M. Bandaru, N. Poojith, S. S. Jadav, M. V. B. Rao, K. S. Babu, R. Sreenivasulu and R. Alluri, *Polycyclic Aromat. Compd.*, 2021, DOI: 10.1080/10406638.2021.1939067.
- 32 A. Ayati, S. Emami, A. Asadipour, A. Shafiee and A. Foroumadi, *Eur. J. Chem.*, 2015, **97**, 699–718.
- 33 P. C. Sharma, A. Jain, M. S. Yar, R. Pahwa, J. Singh and P. Chanaliala, *Arabian J. Chem.*, 2017, **10**, S568–S575.
- 34 B. L. Flynn, G. P. Flynn, E. Hamel and M. K. Jung, *Bioorg. Med. Chem. Lett.*, 2001, **11**, 2341–2343.
- 35 M. S. Al-Said, M. S. Bashandy, S. I. Al-Qasoumi and M. M. Ghorab, *Eur. J. Med. Chem.*, 2011, **46**, 137–141.
- 36 P. Franchetti, L. Cappellacci, M. Grifantini, A. Barzi, G. Nocentini, H. Yang, A. O'Connor, H. N. Jayaram, C. Carrell and B. M. Goldstein, *J. Med. Chem.*, 1995, **38**, 3829–3837.
- 37 X. Li, Y. He, C. H. Ruiz, M. Koenig and M. D. Cameron, *Drug Metab. Dispos.*, 2009, **37**, 1242–1250.
- 38 S. Hu-Lieskován, S. Mok, B. H. Moreno, J. Tsoi, L. Robert, L. Goedert, E. M. Pinheiro, R. C. Koya, T. G. Graeber, B. Comin-Anduix and A. Ribas, *Sci. Transl. Med.*, 2015, **7**, 279ra41.
- 39 M. A. Rashid, K. R. Gustafson, J. H. Cardellina, M. R. Boyd and F. Patellamide, *J. Nat. Prod.*, 1995, **58**, 594–597.
- 40 Y. Yao, S. Chen, X. I. Zhou, L. Xie and A. Chen, *Oncol. Lett.*, 2014, **7**, 541–547.
- 41 K. H. Altmann, *Mini-Rev. Med. Chem.*, 2003, **3**, 149–158.
- 42 S. S. Abd El-Karim, H. S. Mohamed, M. F. Abdelhameed, A. E. Amr, A. A. Almhazia and E. S. Nossier, *Bioorg. Chem.*, 2021, **111**, 104827.
- 43 E. S. Nossier, S. M. El-Hallouty and E. R. Zaki, *Int. J. Pharm. Sci.*, 2015, **7**, 353–359.
- 44 E. S. Nossier, S. S. Abd El-Karim, N. M. Khalifa, A. S. El-Sayed, E. S. Hassan and S. M. El-Hallouty, *Molecules*, 2018, **23**, 3074.
- 45 I. M. Othman, M. A. Gad-Elkareem, A. E. Amr, M. A. Al-Omar, E. S. Nossier and E. A. Elsayed, *J. Enzyme Inhib. Med. Chem.*, 2020, **35**, 1491–1502.
- 46 P. C. Lv, H. Q. Li, J. Sun, Y. Zhou and H. L. Zhu, *Bioorg. Med. Chem.*, 2010, **18**, 4606–4614.
- 47 P. C. Lv, D. D. Li, Q. S. Li, X. Lu, Z. P. Xiao and H. L. Zhu, *Bioorg. Med. Chem. Lett.*, 2011, **21**, 5374–5377.
- 48 M. Y. Zhao, Y. Yin, X. W. Yu, C. B. Sangani, S. F. Wang, A. M. Lu, L. F. Yang, P. C. Lv, M. G. Jiang and H. L. Zhu, *Bioorg. Med. Chem.*, 2015, **23**, 46–54.
- 49 R. Sadashiva, D. Naral, J. Kudva, S. M. Kumar, K. Byrappa, R. M. Shafeeulla and M. Kumsi, *J. Mol. Struct.*, 2017, **1145**, 18–31.
- 50 T. K. Mohamed, R. Z. Batran, S. A. Elseginy, M. M. Ali and A. E. Mahmoud, *Bioorg. Chem.*, 2019, **85**, 253–273.
- 51 K. Vaarla, R. K. Kesharwani, K. Santosh, R. R. Vedula, S. Kotamraju and M. K. Toopurani, *Bioorg. Med. Chem. Lett.*, 2015, **25**, 5797–5803.
- 52 M. O. Sarhan, S. S. Abd El-Karim, M. M. Anwar, R. H. Gouda, W. A. Zagahary and M. A. Khedr, *Molecules*, 2021, **26**, 2273.
- 53 M. M. Anwar, S. S. Abd El-Karim, A. H. Mahmoud, A. E. Amr and M. A. Al-Omar, *Molecules*, 2019, **24**, 2413.
- 54 S. S. Abd El-Karim, Y. M. Syam, A. M. El Kerdawy and T. M. Abdelghany, *Bioorg. Chem.*, 2019, **86**, 80–96.
- 55 A. M. Srouf, N. S. Ahmed, S. S. Abd El-Karim, M. M. Anwar and S. M. El-Hallouty, *Bioorg. Med. Chem.*, 2020, **28**, 115657.
- 56 S. S. Abd El-Karim, M. M. Anwar, E. R. Zaki, S. A. Elseginy and Z. M. Nofal, *Future Med. Chem.*, 2018, **10**, 157–181.
- 57 P. Sharma, S. Kaur, B. S. Chadha, R. Kaur, M. Kaur and S. Kaur, *BMC Microbiol.*, 2021, **21**, 39.
- 58 G. Rodrigues, G. G. Silva, D. F. Buccini, H. M. Duque, S. C. Dias and O. L. Franco, *Front. Microbiol.*, 2019, **10**, 1690.
- 59 V. Patil, K. Tilekar, S. Mehendale-Munj, R. Mohan and C. S. Ramaa, *Eur. J. Med. Chem.*, 2010, **45**, 4539–4544.
- 60 A. E. Amr, R. E. A. Mageid, M. El-Naggar, A. M. Naglah, E. S. Nossier and E. A. Elsayed, *Molecules*, 2020, **25**, 1096.
- 61 E. A. Abd El-Meguid, G. O. Moustafa, H. M. Awad, E. R. Zaki and E. S. Nossier, *J. Mol. Struct.*, 2021, **1240**, 130595.
- 62 L. F. Brown, B. Berse, R. W. Jackman, K. Tognazzi, A. J. Guidi, H. F. Dvorak, D. R. Senger, J. L. Connolly and S. J. Schnitt, *Hum. Pathol.*, 1995, **26**, 86–91.
- 63 A. S. Hassan, G. O. Moustafa, H. M. Awad, E. S. Nossier and M. F. Mady, *ACS Omega*, 2021, **6**, 12361–12374.
- 64 C. Perez, M. Pauli and P. Bazevque, *Acta Biol. Med. Exp.*, 1990, **15**, 113–115.
- 65 A. C. Scott, "Laboratory control of antimicrobial therapy", in *Mackie and MacCartney Practical Medical Microbiology*, ed. J. G. Collee, J. P. Duguid, A. G. Fraser, and B. P. Marmion, Churchill Livingstone, Edinburgh, Scotland, 13th edn, 1989, vol. 2, pp. 161–181.
- 66 Y. M. Syam, M. M. Anwar, E. R. Kotb, S. A. Elseginy, H. M. Awad and G. E. Awad, *Mini-Rev. Med. Chem.*, 2019, **19**, 1255–1275.
- 67 H. E. Hashem, A. E. Amr, E. S. Nossier, E. A. Elsayed and E. M. Azmy, *Molecules*, 2020, **25**, 2766.
- 68 E. M. Mohi El-Deen, E. A. Abd El-Meguid, E. A. Karam, E. S. Nossier and M. F. Ahmed, *Antibiotics*, 2020, **9**, 695.
- 69 E. M. Mohi El-Deen, E. A. Abd El-Meguid, S. Hasabelnaby, E. A. Karam and E. S. Nossier, *Molecules*, 2019, **24**, 3650.
- 70 A. A. El-Sayed, E. S. Nossier, A. A. Almhazia and A. E. Amr, *J. Mol. Struct.*, 2022, **1247**, 131285.



- 71 G. O. Moustafa, A. Shalaby, A. M. Naglah, M. M. Mounier, H. El-Sayed, M. M. Anwar and E. S. Nossier, *Molecules*, 2021, **26**, 4573.
- 72 E. A. Abd El-Meguid, E. M. Mohi El-Deen, G. O. Moustafa, H. M. Awad and E. S. Nossier, *Bioorg. Chem.*, 2021, 105504.
- 73 M. A. Hawata, W. A. El-Sayed, E. S. Nossier and A. A. H. Abdel-Rahman, *Biointerface Res. Appl. Chem.*, 2022, **12**, 5217–5233.
- 74 A. E. G. E. Amr, E. A. Elsayed, M. A. Al-Omar, H. O. Badr Eldin, E. S. Nossier and M. M. Abdallah, *Molecules*, 2019, **24**, 416.
- 75 A. J. King, D. R. Patrick, R. S. Batorsky, M. L. Ho, H. T. Do, S. Y. Zhang, R. Kumar, D. W. Rusnak, A. K. Takle, D. M. Wilson and E. Hugger, *Cancer Res.*, 2006, **66**, 11100–11105.
- 76 *The OSIRIS property explorer software*, available from: <http://www.organic-chemistry.org/prog/peo/>.

